JACS
JOURNAL OF THE AMERICAN CHEMICAL SOCIETY

Article

Potassium-Bromide Surface Passivation on CsPbI3-xBrx Nanocrystals for Efficient and Stable Pure Red Perovskite Light Emitting Diodes

Jun-Nan Yang, Yang Song, Ji-Song Yao, Kun-Hua Wang, Jing-Jing Wang, Bai-Sheng Zhu, Ming-Ming Yao, Sami Ur Rahman, Yi-Feng Lan, Feng-Jia Fan, and Hong-Bin Yao

J. Am. Chem. Soc., **Just Accepted Manuscript** • DOI: 10.1021/jacs.9b11719 • Publication Date (Web): 06 Jan 2020

is published by the American Chemical Society. 1155 Sixteenth Street N.W., Washington, DC 20036

Potassium-Bromide Surface Passivation on $CsPbI_{3-x}Br_x$ Nanocrystals for Efficient and Stable Pure Red Perovskite Light Emitting Diodes

Jun-Nan Yang,[1,2] Yang Song,[1] Ji-Song Yao,[1,2] Kun-Hua Wang,[1,2] Jing-Jing Wang,[1,2] Bai-Sheng Zhu,[2] Ming-Ming Yao,[1,2] Sami Ur Rahman,[1] Yi-Feng Lan,[1] Feng-Jia Fan,[1,3,4] and Hong-Bin Yao*[1,2]

[1]*Hefei National Laboratory for Physical Sciences at the Microscale, University of Science and Technology of China, Hefei, Anhui 230026, China*

[2]*Department of Applied Chemistry, Hefei Science Center of Chinese Academy of Sciences, University of Science and Technology of China, Hefei, Anhui 230026, China*

[3]*CAS Key Laboratory of Microscale Magnetic Resonance, University of Science and Technology of China, He fei, Anhui 230026, China*

[4]*Synergetic Innovation Center of Quantum Information and Quantum Physics, University of Science and Tech nology of China, Hefei, Anhui 230026, China*

* Corresponding author Email: yhb@ustc.edu.cn

ABSTRACT

All-inorganic lead halide perovskite nanocrystals (NCs) are potential candidates for fabricating high-performance light-emitting diodes (LEDs) owing to their precise tunable bandgaps, high photoluminescence (PL) efficiency and excellent color purities. However, the performance of pure red (630 ~ 640 nm) all-inorganic perovskite LEDs is still limited by the halide segregation-induced instability of the electroluminescence (EL) of mixed halide $CsPbI_{3-x}Br_x$ NCs. Herein, we report an effective approach to improving the EL stability of pure red all-inorganic $CsPbI_{3-x}Br_x$ NC-based LEDs via the passivation of potassium bromide on NCs. By adding potassium oleate to the reaction system, we obtained potassium bromide surface passivated (K-Br passivated) $CsPbI_{3-x}Br_x$ NCs with pure red PL emission and a photoluminescence quantum yield (PLQY) exceeding 90%. We determine that most potassium ions present on the surface of NCs bind with bromide ions and thus demonstrate that potassium bromide surface passivation of NCs can both improve the PL stability and inhibit the halide segregation of NCs. Using K-Br-passivated $CsPbI_{3-x}Br_x$ NCs as an emitting layer, we fabricated stable and pure red perovskite LEDs with emission at 637 nm, showing a maximum brightness of 2671 cd m^{-2}, maximum external quantum efficiency of 3.55%, and good EL stability. The proposed K-Br-passivated NC strategy will open a new avenue for fabricating efficient, stable and tunable pure color perovskite NC LEDs.

Keywords: metal halide perovskite, nanocrystals, light emitting diode, segregation, stability

INTRODUCTION

In the past few years, incredible advances have been made in improving the performance of all-inorganic lead halide perovskite-based light-emitting diodes (LEDs).[1, 2] The excellent properties of all-inorganic lead halide perovskites, such as high PLQY,[3] narrow full-width at half-maximum (FWHM),[4] and ease of bandgap tuning,[5] make them next-generation materials for LED displays. While the external quantum efficiency (EQE) exceeds 20% for green emitters based on $CsPbBr_3$/MABr quasi-core/shell structures[6] and red emitters based on anion-exchanged $CsPbI_{3-x}Br_x$ NCs[7] and near-infrared emitters based on 2,2′-[oxybis(ethylenoxy)]-diethylamine-treated $FAPbI_3$ perovskite layers[8] have been reported, the performance of pure red emitters (630 ~ 640 nm) needs to be improved to meet application requirements.[9] This is because the red channel for a display centered at the 630 nm emission peak wavelength (Rec. 2020) is a key target to realize the practical application of LEDs for displays.[10]

Mixed halide $CsPbI_{3-x}Br_x$ NCs emitting in the range of 630 ~ 640 nm are promising candidate materials for pure red LEDs.[11] However, under photoirradiation or with an applied bias, the emission peak of mixed halide perovskites will present a blueshift or redshift due to the segregation of halide ions; that is, mixed halide phases are divided into two separated halide phases.[12-14] Typically, by applying a bias voltage on $CsPbI_{3-x}Br_x$ NC-based LEDs, the mixed phases are divided into higher-bandgap bromide-rich domains and lower-bandgap iodide-rich domains on account of the different ionic mobilities of bromide ions and iodide ions.[11] After that, subsequent light emission occurs from these iodide-rich domains due to their favorable band offsets.[15] Consequently, the EL emission peak exhibits a redshift,

resulting in the low stability of the EL spectra of pure red $CsPbI_{3-x}Br_x$ NC-based LEDs. To date, the Junji Kido group demonstrated the highest EQEs of pure red perovskite LEDs emitting at 653 nm based on anion-exchanged $CsPbI_{3-x}Br_x$ NCs,[7] but the retention of red color purity in the as-fabricated LEDs is still a critical issue.[9]

To minimize photoinduced halide segregation in mixed halide perovskites, several strategies have recently been proposed and investigated in solar cells,[16] including (i) incorporating other cations into the A site of the perovskite matrix to increase the entropic contributions of phase segregation,[17] (ii) increasing the crystalline size by substituting Pb^{2+} with Sn^{2+} cations into the B site of the perovskite matrix,[18] and (iii) passivating the surface of perovskites with potassium cations to form a potassium-halide layer to suppress photoinduced ion migration in perovskite polycrystalline films.[19] However, for LEDs, the crystalline size of perovskites has to be confined at the nanoscale for efficient light emission, and the ion migration caused by an electric field is more serious than the photoinduced ion migration in solar cells, making it more difficult to stabilize the EL peak of mixed halide perovskite-based LEDs. To suppress halide segregation in perovskite LEDs, passivation of the surface halide vacancies in mixed halide nanocrystalline perovskites is required to inhibit ion migration because the surface halide vacancies that trigger ion migration are suppressed.[20] In addition, tuning the crystalline size below the threshold size (approximately 46 nm) is a possible route to fabricate phase-segregation-free mixed halide perovskite films by counterbalancing the confinement of carrier diffusion into the grains with the formation and accumulation of segregated domains.[21] Last but not least, modifying the grain boundary of perovskite polycrystals with a passivated potassium-halide layer can both significantly improve the

optical properties and suppress the ion migration of a perovskite polycrystalline film, which has potential application prospects for stabilizing the EL of light emitting diodes.[19] Thus, a new type of well-passivated mixed halide perovskite $CsPbI_{3-x}Br_x$ NCs are desirable as emitters for pure color, stable perovskite LEDs.

Based on the above strategies,[19-22] herein, we report the preparation of high-quality potassium bromide surface passivated (K-Br passivated) mixed halide perovskite $CsPbI_{3-x}Br_x$ NCs for the fabrication of stable and pure red perovskite LEDs. The synthesis of passivated NCs is facilely achieved via a typical hot-injection (HI) method by adding K-oleate (K-OA) to the precursor solution and then swiftly injecting a mixture of trimethylsilyl bromine (TMSBr) and trimethylsilyl iodide (TMSI) at 180 °C.[23] The obtained K-Br-passivated $CsPbI_{3-x}Br_x$ NCs exhibited a high PLQY (over 90%), high dispersibility, and good stability for weeks under ambient conditions. We fabricated pure red perovskite LEDs emitting at 637 nm using the obtained K-Br-surface-passivated $CsPbI_{3-x}Br_x$ NC film as an emitter, and the maximum EQE of the device reached 3.55%. Importantly, K-Br-passivated $CsPbI_{3-x}Br_x$ NC-based pure red LEDs showed high color stability during the operation.

EXPERIMENTAL SECTION

Chemicals. Cesium acetate (CH_3COOCs, Aladdin, 99.99%), lead acetate trihydrate ($Pb(CH_3COO)_2{\cdot}3H_2O$, Aladdin, 99.998%), potassium acetate (CH_3COOK, Macklin, 99.0%, AR), sodium acetate (CH_3COONa, Aladdin, AR), lithium acetate (CH_3COOLi, Aladdin, 99%), 1-octadecene (ODE, Aldrich, 90%), oleylamine (OAm, Aldrich, 70%), oleic acid (OA, Afla Aesar, 90%), trimethylsilyl iodide (TMSI, Aladdin, 97%, with Cu as a stabilizer),

trimethylsilyl bromine (TMSBr, Aladdin, 98%, with Cu as a stabilizer), PEDOT:PSS solution (Al4083 CLEVIOS), poly-TPD (Xi'an Polymer Light Technology Corp.), TPBi (Nichem), toluene (C_7H_8, Sinopharm Chemical Reagent Co. Ltd. (SCRC), AR), n-octane (C_8H_{18}, SCRC, AR), ethyl acetate ($CH_3COOCH_2CH_3$, SCRC, AR), and methyl acetate (CH_3COOCH_3, Aladdin, 99.5%, anhydrous) were used without further purification.

Material Synthesis. *Preparation of K-oleate:* The K-oleate (K-OA) precursor was prepared by loading a mixture of 0.1 mmol of CH_3COOK, 4.5 mL of ODE and 0.5 mL of OA into a 7 mL vial. Then, the solution was heated and stirred for 30 min at 80 °C to form a transparent solution. The obtained K-OA solution was stored in dry conditions. The concentration of K-OA in the solution was 0.02 mol L^{-1}.

Preparation of Li-oleate: The Li-oleate (Li-OA) precursor was prepared by loading a mixture of 0.1 mmol of CH_3COOLi, 4.5 mL of ODE and 0.5 mL of OA into a 7 mL vial. Then, the solution was heated and stirred for 30 min at 80 °C to form a transparent solution. The obtained Li-OA solution was stored in dry conditions. The concentration of Li-OA in the solution was 0.02 mol L^{-1}.

Preparation of Na-oleate: The Na-oleate (Na-OA) precursor was prepared by loading a mixture of 0.1 mmol of CH_3COONa, 4.5 mL of ODE and 0.5 mL of OA into a 7 mL vial. Then, the solution was heated and stirred for 30 min at 80 °C to form a transparent solution. The obtained Na-OA solution was stored in dry conditions. The concentration of Na-OA in the solution was 0.02 mol L^{-1}.

Synthesis of pristine $CsPbI_{3-x}Br_x$ NCs: First, 0.1 mmol of CH_3COOCs, 0.2 mmol of $Pb(CH_3COO)_2 \cdot 3H_2O$ and 5 mL of ODE were added into a 25 mL 3-neck flask, and the

obtained solution was degassed under vacuum for 20 min at 120 °C and then placed under nitrogen flow for 5 min. Then, 0.5 mL of OA and 1.0 mL of OAm were injected into the above solution under nitrogen flow. Five minutes later, the flask was placed under vacuum again for 30 min until the solution was transparent and clear. Subsequently, the temperature was increased to 180 °C under nitrogen flow, and a mixture of 58 μL of TMSBr and 110 μL of TMSI was swiftly injected. After at least 10 s, the reaction mixture was cooled in an ice-water bath.

Synthesis of K-Br-passivated $CsPbI_{3-x}Br_x$ NCs: First, 0.1 mmol of CH_3COOCs, 0.2 mmol of $Pb(CH_3COO)_2 \cdot 3H_2O$, 1.0 mL of K-OA and 4.0 mL of ODE were added into a 25 mL 3-neck flask. The remaining synthetic procedure was the same as above. Notably, the ratio of K to Pb was 10% in our typical synthesis.

Synthesis of Li-passivated $CsPbI_{3-x}Br_x$ NCs: First, 0.1 mmol of CH_3COOCs, 0.2 mmol of $Pb(CH_3COO)_2 \cdot 3H_2O$, 1.0 mL of Li-OA and 4.0 mL of ODE were added into a 25 mL 3-neck flask. The remaining synthetic procedure was the same as above. Notably, the ratio of Li to Pb was 10% in our typical synthesis.

Synthesis of Na-passivated $CsPbI_{3-x}Br_x$ NCs: First, 0.1 mmol of CH_3COOCs, 0.2 mmol of $Pb(CH_3COO)_2 \cdot 3H_2O$, 1.0 mL of Na-OA and 4.0 mL of ODE were added into a 25 mL 3-neck flask. The remaining synthetic procedure was the same as above. Notably, the ratio of Na to Pb was 10% in our typical synthesis.

Purification of Prepared $CsPbI_{3-x}Br_x$ NCs: The obtained NCs in crude solution were precipitated by adding ethyl acetate (volume ratio to that of the NC solution of 3:1), and then, the mixture was centrifuged at 10000 rpm for 10 min. The supernatant was discarded, and the

precipitate was redispersed in 3.0 mL of toluene. The solution was further centrifuged for 3 min at 3000 rpm, and the supernatant was retained. Additional washing could be conducted by adding methyl acetate (volume ratio to that of the NC solution of 3:1) for 5 min at 10000 rpm to precipitate the NCs. Finally, the obtained precipitate was redispersed in 1.5 mL of n-octane for subsequent characterizations and tests.

$CsPbI_{3-x}Br_x$ NC-Based LED Fabrication and Performance Test. Initially, the ITO glass substrate was ultrasonically cleaned in ITO washing solution, deionized water, isopropyl alcohol, acetone and ethanol in sequence. After that, the substrate was dried with nitrogen flow and treated by UV-ozone for 20 min. After the surface treatment, the PEDOT:PSS solution was spun onto the surface of the ITO-coated glass substrate by a spin coater (Chemat Technology spin-coater kw-4A) at 3000 rpm for 50 s and annealed at 140°C on a hot plate (Chemat Technology kw-4AH) for 15 min under ambient conditions. A solution of poly-TPD in chlorobenzene (8 mg mL^{-1}) was spin-coated on the PEDOT:PSS layer by a spin-coater at 3000 rpm for 50 s and annealed at 130 °C on a hot plate for 30 min under a nitrogen atmosphere. To form an NC emission layer, the NC solution was spin-coated on top of the poly-TPD film at a speed of 2000 rpm for 45 s. Finally, 40 nm TPBI, 1 nm LiF and 100 nm Al were thermally evaporated under a high vacuum (~2×10^{-4} Pa). The device active area was 4 mm^2. For the as-fabricated LED device performance test, a Keithley 2400 SourceMeter was used to record the current versus voltage characteristics. The luminescence of the device was revealed by photon flux using a silicon photodiode, which was calibrated by a PR-670 spectra scan luminance meter. The electroluminescent spectrum (EL) of the device was collected using an Ocean Optics JAZ spectrometer. Other important parameters used to

characterize LEDs were all calculated from the L-J-V and EL measurements under the assumption that the emission of the LED exhibits a Lambertian pattern. The performance measurement for the device was carried out under a nitrogen atmosphere in a glove box at room temperature without any encapsulation.

Characterizations. Transmission electron microscopy (TEM) analysis was performed on a Hitachi HT-7700 operating at an accelerating voltage of 100 kV. The high-resolution TEM (HRTEM) and high-angle annular dark field scanning transmission electron microscopy (HAADF-STEM) images were carried out by a Talos F200X operating at an accelerating voltage of 200 kV. The energy dispersive X-ray spectroscopy (EDS) spectra were collected on a Talos F200X with an energy dispersive detector. The scanning electron microscopy (SEM) images were taken on a JEOL-JSM-6700 scanning electron microscope at an acceleration voltage of 5 kV. The atomic force microscopy (AFM) images were collected by using a Veeco DI Nanoscope V system with tapping mode. The powder X-ray diffraction (PXRD) pattern analysis was acquired by a Philips X'Pert PRO SUPER X-ray diffractometer using Cu Kα radiation (λ = 1.54178 Å). The elemental analysis was carried out on a PerkinElmer Optima 7300 DV inductively coupled plasma-optical emission spectrometer (ICP-OES). X-ray photoelectron spectroscopy (XPS) was conducted on NCs loaded on a silicon wafer by a Thermo ESCALAB 250 spectrometer equipped with a monochromatic Al Kr radiation source (1486.7 eV). The ultraviolet-visible (UV-vis) absorption spectra of the NC solution were measured by using a PekinElmer instrument in transmission mode. The PL spectra and PLQYs were measured on a Hamamatsu (C11347) absolute PLQY spectrometer using 365 nm excitation on diluted toluene suspensions in a quartz cuvette. The UV-vis

absorption spectra were recorded using a Varian Cary 300 UV-vis absorption spectrophotometer. The Fourier transform infrared spectra (FT-IR) of NC powders were obtained with a potassium bromide pellet by Nicolet 8700. ^{1}H nuclear magnetic resonance (^{1}H NMR) spectroscopy was acquired by Bruker AVANCE AV III 400. The NMR spectra of the samples were measured using ferrocene as an internal standard. In brief, a mixture of perovskite NCs and ferrocene (9:1 wt/wt) in deuterated chloroform was prepared at a concentration of 10 mg ml^{-1} for ^{1}H NMR measurements. Time-resolved PL measurements were obtained with our home-built time-correlated single photon counting (TCSPC) system under ambient conditions. The $CsPbI_{3-x}Br_x$ NC solution stored in a 1 cm cuvette and the $CsPbI_{3-x}Br_x$ NC film spin-coated on the glass substrate were excited using a 405 nm laser (Picosecond Diode Laser, PiLas). The synchrotron radiation photoemission spectroscopy (SRPES) experiments were performed at the photoemission end-station at beamline BL10B in the Hefei National Synchrotron Radiation Laboratory. In the current work, SRPES spectra were taken with synchrotron photon energy levels of 450 eV, 650 eV and 1486.7 eV.

RESULTS AND DISCUSSION

Potassium bromide-passivated $CsPbI_{3-x}Br_x$ NC synthesis and characterization

For the synthesis of all $CsPbI_{3-x}Br_x$ NCs, we used an HI method with TMSBr and TMSI as the halogen source (see the experimental section for details).[23] We adopted an excessive halogen source to obtain halide-rich NCs (molar ratio of Pb to X of 1:6).[24] For the K-Br-passivated $CsPbI_{3-x}Br_x$ NCs, we added 1.0 mL of K-OA (0.02M) into the precursor solution before adding oleic acid (OA) and oleylamine (OAm), in which the molar ratio of K

to Pb was 10%. Notably, unless otherwise stated, all the samples were purified twice before measurement. Figure 1a shows the transmission electron microscopy (TEM) image of the as-synthesized K-Br-passivated $CsPbI_{3-x}Br_x$ NCs, demonstrating their monodispersity and cubic shape, as expected for Cs-based lead halide perovskite NCs.[4] The typical high-resolution TEM (HRTEM) image of K-Br-passivated $CsPbI_{3-x}Br_x$ NCs is shown as the inset in Figure 1a. As a comparison, the TEM and HRTEM images of pristine $CsPbI_{3-x}Br_x$ NCs are provided in Figure S1. Obviously, the lattice distances of both NCs are 0.30 nm, corresponding to the (200) plane lattice spacing of cubic phase $CsPbI_{3-x}Br_x$.[25] The size distribution of NCs was counted based on the TEM image, and both samples showed almost the same average size of approximately 11.4 nm (Figure S2), indicating that the addition of potassium ions did not obviously affect the crystalline size of NCs. Moreover, the spatial distributions of Cs, Pb, I, Br and K species in K-Br passivated $CsPbI_{3-x}Br_x$ NCs were further revealed by high-angle annular dark field scanning transmission electron microscopy (HAADF-STEM) and corresponding elemental mapping (Figure 1b). The homogeneous distribution of main elements (Cs, Pb, I and Br) among all of the NCs suggests that halogens are mixed well in the perovskite lattice, and the distribution of potassium in the spatial region indicated that potassium ions were present in the $CsPbI_{3-x}Br_x$ NCs. Energy dispersive X-ray spectroscopy (EDS) elemental quantification revealed a Cs: Pb: I: Br: K atomic ratio of 1.05: 1.00: 1.84: 0.90: 0.05 (Figure S3). Elemental scan profiles of potassium and lead elements (Figure 1c) further present that the signal of potassium for a typical NC displayed relatively high counts, implying that potassium ions mainly exist on the surface of the $CsPbI_{3-x}Br_x$ NCs.[22]

To further validate the location of the potassium ions, we applied X-ray diffraction (XRD) patterns (Figure 1d) to obtain more information on the crystal structure of the as-prepared $CsPbI_{3-x}Br_x$ NCs. Both NCs have cubic crystalline structures (refer to α-$CsPbI_3$ ICSD No.161481) and no formation of any impurity phases. Careful examination of the XRD patterns reveals that the peak intensity of the K-Br-passivated $CsPbI_{3-x}Br_x$ NCs is stronger than that of the pristine $CsPbI_{3-x}Br_x$ NCs, which verifies that the addition of potassium ions can improve the crystallinity of the NCs. Furthermore, we determined the atomic ratio of K to Pb in K-Br-passivated $CsPbI_{3-x}Br_x$ NCs by inductively coupled plasma-optical emission spectroscopy (ICP-OES) (Table S1). For the sample with one cycle of purification by ethyl acetate, the ratio of K to Pb was 10.6%. After two cycles of purification by methyl acetate,[26] the ratio of K to Pb decreased to 6.0%, which well matched the elemental quantification measured by EDS. In this context, we speculate that the potassium ions were enriched on the surface of the NCs.[19, 22]

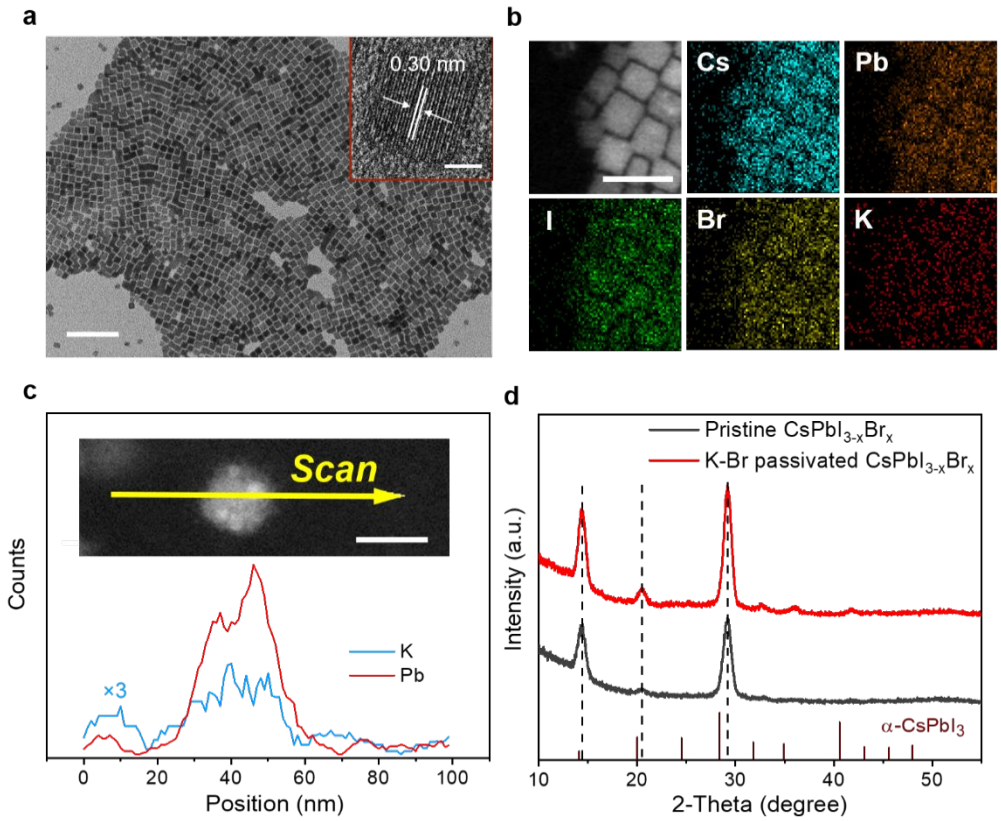

Figure 1. Morphology and characterizations of the as-synthesized K-Br-passivated $CsPbI_{3-x}Br_x$ NCs. (a) The TEM image of K-Br-passivated $CsPbI_{3-x}Br_x$ NCs. The inset shows the corresponding HRTEM image. Scale bars: 100 nm and 5 nm, respectively. (b) HAADF-STEM image and corresponding elemental mapping images of K-Br-passivated $CsPbI_{3-x}Br_x$ NCs. Scale bar: 20 nm. (c) Elemental scan profiles of potassium and lead from a typical single NC as indicated by the yellow arrow in the dark-field STEM image. The counts of the potassium element signal are tripled. Scale bar: 20 nm. (d) XRD patterns of the prepared $CsPbI_{3-x}Br_x$ NCs (α-$CsPbI_3$ ICSD No.161481).

To figure out the states of the potassium ions present on the surface of the NCs, the high--resolution XPS spectra are provided in Figure 2a and Figure S5. All elements, Cs 3*d*, Pb 4*f*, I 3*d*, Br 3*d* and K 2*p* for the pristine $CsPbI_{3-x}Br_x$ NCs and K-Br-passivated $CsPbI_{3-x}Br_x$ NCs were calibrated with C 1s. The signal of potassium was detected after the addition of K-OA, which further proved the existence of K on the surface of the NCs. In addition, after adding K-OA, the Br $3d_{3/2}$ and $3d_{5/2}$ peaks shifted to higher binding energies from 69.3 and 68.3 eV to 69.6 and 68.5 eV, respectively, while the Pb $4f_{5/2}$ and $4f_{7/2}$ peaks at 143.2 and 138.3 eV slightly shifted to lower binding energies of 143.1 and 138.2 eV. Concurrently, no obvious

peak shift was observed for I 3*d* and Cs 3*d* spectra. We inferred that these results could be attributed to the strong bond between potassium ions and bromide ions on the surface of the NCs, which also weakened the bond between lead ions and bromide ions.

To further confirm that the most of potassium ions present on the surface of the NCs were bonded with bromide ions, we used synchrotron radiation photoemission spectroscopy (SRPES) characterization on the uniform K-Br-passivated $CsPbI_{3-x}Br_x$ NC film spin-coated on a silicon substrate. Utilizing incident photons with different energies can detect the elementary information about the NC film at different thicknesses because the higher energy photons can deeper penetrate the NCs and the detecting thickness is usually less than the size of a single NC (Figure 2b).[27] First, the SRPES spectra were taken with synchrotron photon energy levels of 450 eV and 650 eV under a nitrogen atmosphere. As shown in Figure 2c, when the energy of the incident photons was 450 eV, the ratio of K: Br: Pb on the surface of the $CsPbI_{3-x}Br_x$ NC film was calculated to be 0.141: 1.96: 1. In contrast, the ratio of K: Br: Pb decreased to 0.085: 1.14: 1 when the energy of incident photons increased to 650 eV (Figure 2d). These results show that, as the detection depth increased, the ratio of K and Br to Pb decreased significantly, which indicates that the potassium ions and bromide ions are enriched on the surface of the $CsPbI_{3-x}Br_x$ NCs. We further enhanced the incident photon energy to 1486.7 eV using a monochromatic Al Kr radiation source in order to detect deeper elementary information in the $CsPbI_{3-x}Br_x$ NCs. As the energy of incident photons increased to 1486.7 eV, the ratio of K: Br: Pb was calculated to be 0.101: 1.19: 1 (Figure 2e). The slight increase in the ratio of K and Br to Pb can be attributed to the detection thickness variation and the inhomogeneous distribution of potassium ions and bromide ions across the section of NCs.

Furthermore, we compared the binding energy variation of Pb, K and Br at a different detection depth to reveal the binding type of Pb, Br and K on the surface and inside of the NC. The binding energy of Br 3*d* and K 2*p* decreased as the depth of detection increased (Figure 2f and Figure 2g), while no obvious peak shift was observed for the Pb 4*f* spectrum (Figure 2h), indicating that bromide and potassium have different bonding types on the surface and in the interior of NCs. The reduction in the internal binding energy of bromide comes from the stronger bond between bromide ions and potassium ions than that between bromide ions and lead ions (68.70 eV for Br $3d_{5/2}$ of KBr and 68.10 eV for Br $3d_{5/2}$ of $CsPbBr_3$).[28, 29] Additionally, the decreasing internal binding energy of potassium results from the fact that potassium ions enter the interstitial area of the perovskite lattice in the NCs. Therefore, we confirmed that the potassium ions were not only enriched on the surface of NCs binding with bromide ions but also entered the perovskite lattice in a small amount.

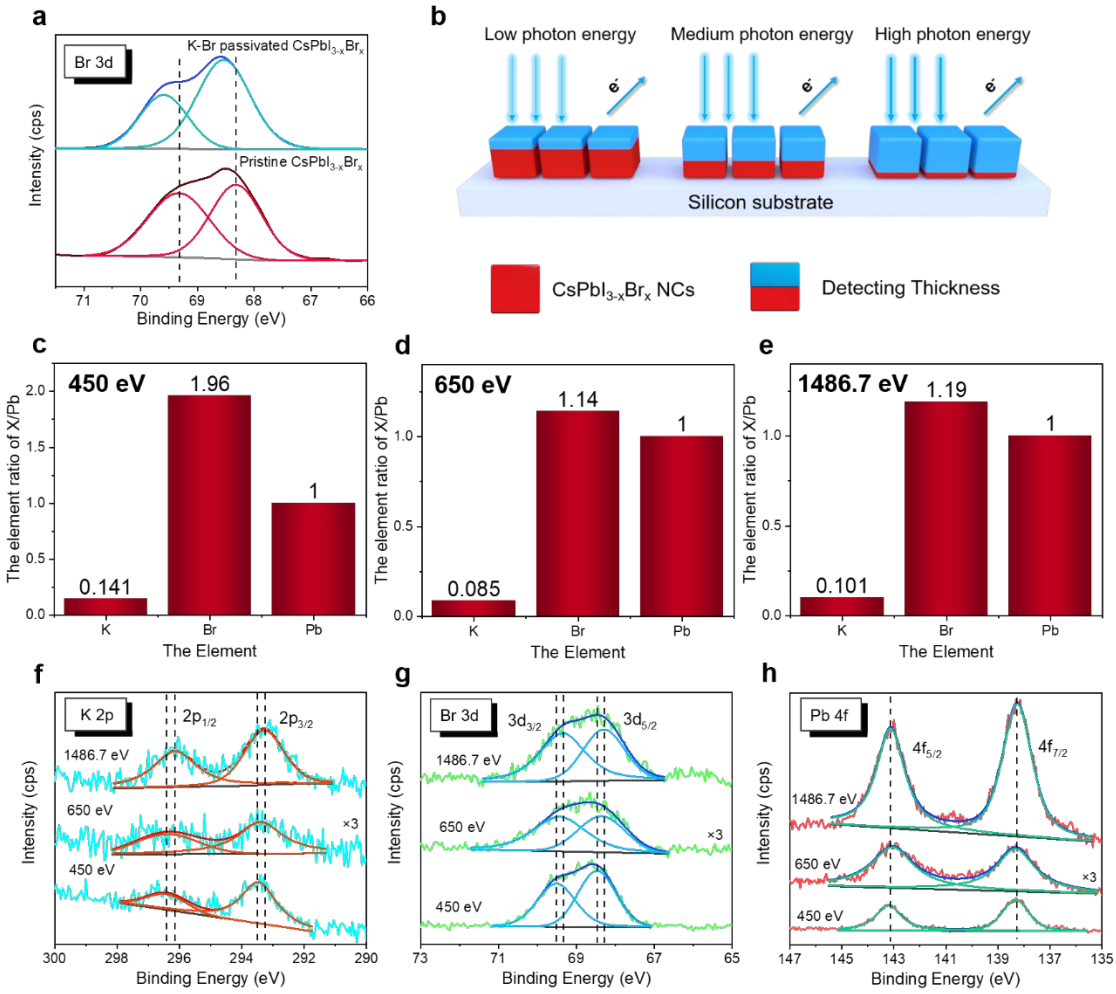

Figure 2. X-ray photoelectron spectroscopy characterizations of $CsPbI_{3-x}Br_x$ NCs. (a) High-resolution XPS spectra of pristine and K-Br-passivated $CsPbI_{3-x}Br_x$ NCs for Br 3*d*. (b) Schematic illustration of SRPES detected with photons of different energy levels. Photons with higher energy can detect thicker-scale elemental information in the NC film. (c-e) The atomic ratios of X/Pb measured by SRPES for K-Br-passivated $CsPbI_{3-x}Br_x$ NC film with photons of different energy levels. (c) 450 eV, (d) 650 eV and (e) 1486.7 eV. (f-h) The SRPES of K-Br-passivated $CsPbI_{3-x}Br_x$ NC film for (f) K 2*p*, (g) Br 3*d* and (h) Pb 4*f*. The energy levels of incident photons are 450 eV, 650 eV and 1486.7 eV, respectively. The intensity of the sample measured by photons with an energy of 650 eV tripled.

In addition, we characterized the optical properties of prepared mixed halide perovskite NC solutions. Figure 3a shows the NC solution under daylight and UV light, and both samples are well dispersed with bright pure red emission. PL spectra and UV-vis absorption of these prepared NC solutions are exhibited in Figure 3b, and the emission peaks of both $CsPbI_{3-x}Br_x$

NCs are approximately 640 nm. The PLQY of K-Br-passivated $CsPbI_{3-x}Br_x$ NCs was maintained at 93% even after two cycles of purification, signifying the good surface passivation effect for K-Br enriched on the surface of $CsPbI_{3-x}Br_x$ NCs. Time-resolved PL decay curves of these prepared NC solutions are presented in Figure 3c and Figure S7. The PL decay curves were fitted with a biexponential function to determine the PL decay lifetimes, which are summarized in Table S2 and Table S3. The PL lifetime of K-Br-passivated $CsPbI_{3-x}Br_x$ NCs (30.51 ns) is similar to that of pristine $CsPbI_{3-x}Br_x$ NCs (29.02 ns), due to the low defect concentration induced by the halide-rich surface of both samples in solution (Figure S8).

The surface organic ligands of NCs prefer to block charge injection and transport inside LEDs due to the poor electrical conductivity of OA and OAm.[7, 30] The Fourier transform infrared spectra (FT-IR) were used to examine the presence of ligands on the surface of the as-synthesized $CsPbI_{3-x}Br_x$ NCs (Figure S9). The FT-IR characterizations present peaks located at 2926 and 2853 cm^{-1} ascribed to the C-H stretching modes of alkyl groups, which exhibit an obvious decrease with further purification. However, after two cycles of purification, the FT-IR peaks located at 1698 cm^{-1} and 1632 cm^{-1} belonging to the C=O and $N\text{-}H_3^+$ stretching modes still exist, indicating that a small amount of OA and OAm still exist on the surface of the NCs to stabilize the NCs.[30] We also tested the ^1H NMR spectra of the samples using ferrocene as an internal standard to determine the contents of OA and OAm.[7] All ^1H NMR signals from the NCs were normalized using the ferrocene resonance (4.19 ppm) as the reference. As shown in Figure 3d, the intensity of the alkenyl region (δ = 5.2-5.4 ppm) of the ^1H NMR spectra obviously decreased, signifying that the total concentration of surface

ligands decreased after further purification, which is consistent with the FT-IR characterization. There is no manifest difference between pristine $CsPbI_{3-x}Br_x$ NCs and K-Br-passivated $CsPbI_{3-x}Br_x$ NCs in terms of surface ligands, demonstrating that K-Br surface passivation did not affect the condition of the surface ligands.

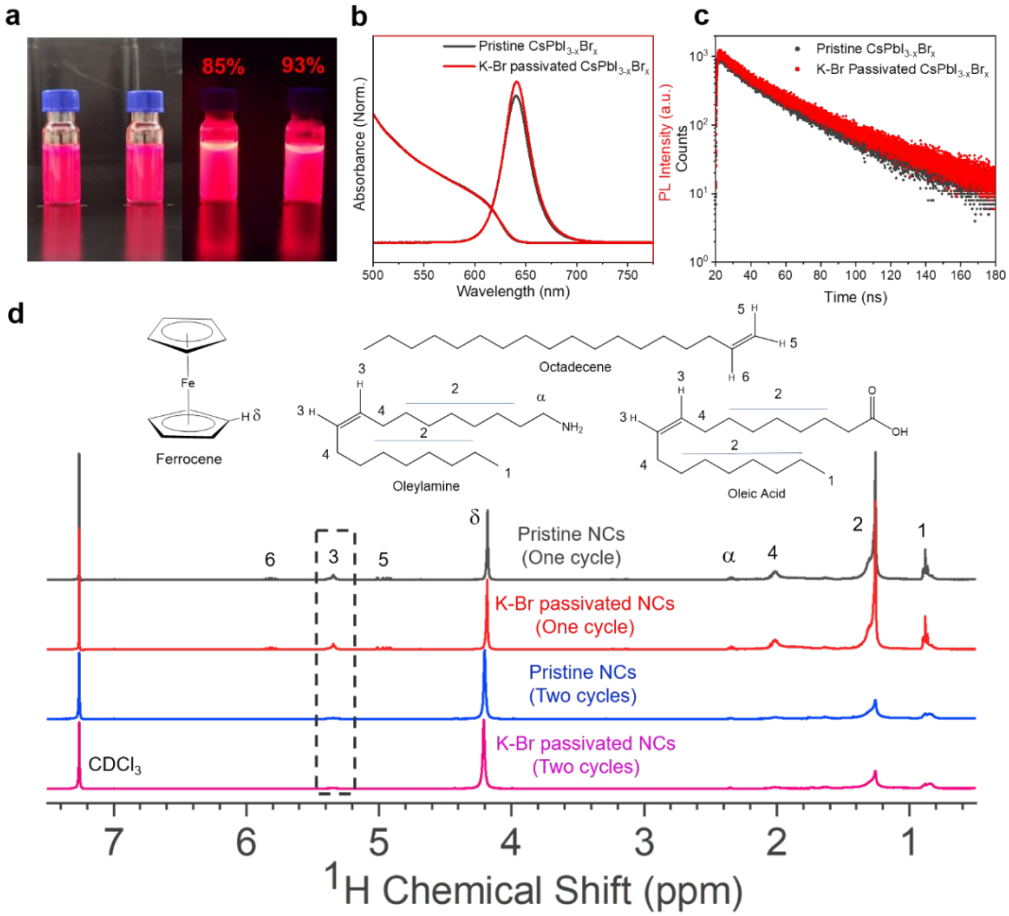

Figure 3. Characterization of prepared NC solutions. (a) Photos of prepared $CsPbI_{3-x}Br_x$ NC solutions under daylight (left) and UV-light (365 nm) irradiation (right). The left sample is the pristine $CsPbI_{3-x}Br_x$ NC solution, and the right sample is the K-Br-passivated $CsPbI_{3-x}Br_x$ NC solution. The PLQYs of these two samples were 85% and 93%, respectively. (b) Absorbance and PL spectra of the prepared $CsPbI_{3-x}Br_x$ NC solution. (c) Time-resolved PL spectra of the prepared $CsPbI_{3-x}Br_x$ NC solution. (d) ^1H NMR spectroscopy of pristine $CsPbI_{3-x}Br_x$ NCs and K-Br-passivated $CsPbI_{3-x}Br_x$ NCs with different purification cycles. A certain amount of ferrocene was added in the solution as an internal standard.

It should be noted that excessive potassium ions in the reaction solution have an adverse effect on the morphology and structure of NCs. The TEM images of different ratios of K to

Pb in the reaction solution are provided in Figure S10. When the ratio of K to Pb is over 20%, the $CsPbI_{3-x}Br_x$ NCs are easily aggregated, and some large fused crystals are formed. Correspondingly, impurity phase $KBr_{0.67}I_{0.33}$ (ICSD No.24-1117) was detected in the products of the 20% and 30% K^+ reaction systems, while no impurity phase was discovered in the 10% K^+ $CsPbI_{3-x}Br_x$ NCs (Figure S11). This phenomenon illustrates that potassium ions have strong bonding with excessive halide ions, especially bromide ions, on the surface of NCs. Simultaneously, when the ratio of K to Pb reached 20%, the bond between excess potassium ions and surface halide ions will increase the halide vacancies on the surface of the NCs, leading to the decrease in the PLQY (Figure S12) and the reduction in the NC solution stability (Figure S13 and Figure S14).[22] Therefore, the appropriate ratio of K to Pb is necessary to gain well-passivated $CsPbI_{3-x}Br_x$ NCs.

Moreover, we synthesized a series of other alkali metal ion-passivated $CsPbI_{3-x}Br_x$ NCs (Li and Na) by adding 0.02 mmol of Li-OA or 0.02 mmol of Na-OA to the reaction system, and the ratio of alkali metal ion to lead is 1: 10. However, after storage in air for ten days, the PLQYs of the Li- and Na-passivated NC solutions showed apparent decreased (Figure S15). In addition, after storage in air, a large number of fused particles formed in the Li-passivated $CsPbI_{3-x}Br_x$ NCs, and a small amount of agglomerated particles formed in the Na-passivated $CsPbI_{3-x}Br_x$ NCs, as shown in the TEM images (Figure S16), indicating that lithium ions and sodium ions exhibited a limited passivation effect on $CsPbI_{3-x}Br_x$ NCs.

Stable, pure red emissive $CsPbI_{3-x}Br_x$ NC films

We further fabricated $CsPbI_{3-x}Br_x$ NC solid thin films via spin-coating and characterized

their optical properties and stabilities. By spin-coating NC solution on the clean glass substrates, we obtained smooth thin films with high PLQYs (Figure 4a). The PL emission of the as-obtained films shows a slight redshift (~1-2 nm) compared with the initial emissions from NC solution due to formation of conduction/valence bands through agglomeration of NCs (Figure 4b).[21] Similarly, the time-resolved PL decay curves of these prepared NC films tested in air are presented in Figure 4c. The PL decay curves were fitted with a biexponential function to determine the PL decay lifetimes, which are summarized in Table S4. It has been demonstrated that surface defects will give rise to nonradiative surface states and lead to shorter exciton lifetimes.[31] The PL lifetime of K-Br-passivated $CsPbI_{3-x}Br_x$ NC film (21.11 ns) is longer than that of the pristine $CsPbI_{3-x}Br_x$ NC film (15.84 ns), signifying that the K-Br-passivated $CsPbI_{3-x}Br_x$ NC film possesses fewer trap states and has better pure red light emission.[32] It should be noted that, in the pristine $CsPbI_{3-x}Br_x$ NC film, moisture attack on the surface of pristine NCs causes the formation of defects when they are exposed to air without the protection of a solvent, and these defects can trap excitons, resulting in more nonradiative recombination (Figure S17a).[33] However, in the K-Br-passivated NC film, the defect concentration on the surface is lower than that of the pristine NC films due to the passivation effect of the K-Br enriched surface, leading to less nonradiative recombination and a longer PL lifetime (Figure S17b). In addition, we tested the PL lifetime of NC films exposed to air for 30 min to show the effect of K-Br surface passivation (Figure S18 and Table S4). The PL lifetimes of freshly prepared and aged K-Br-passivated $CsPbI_{3-x}Br_x$ NC films are 21.11 and 20.70 ns, respectively. In contrast, the PL lifetimes of freshly prepared and aged pristine $CsPbI_{3-x}Br_x$ NC films are 15.84 and 11.57 ns, respectively. These results indicate that K-Br

passivation can provide better protection for an NC film to maintain PL in air.

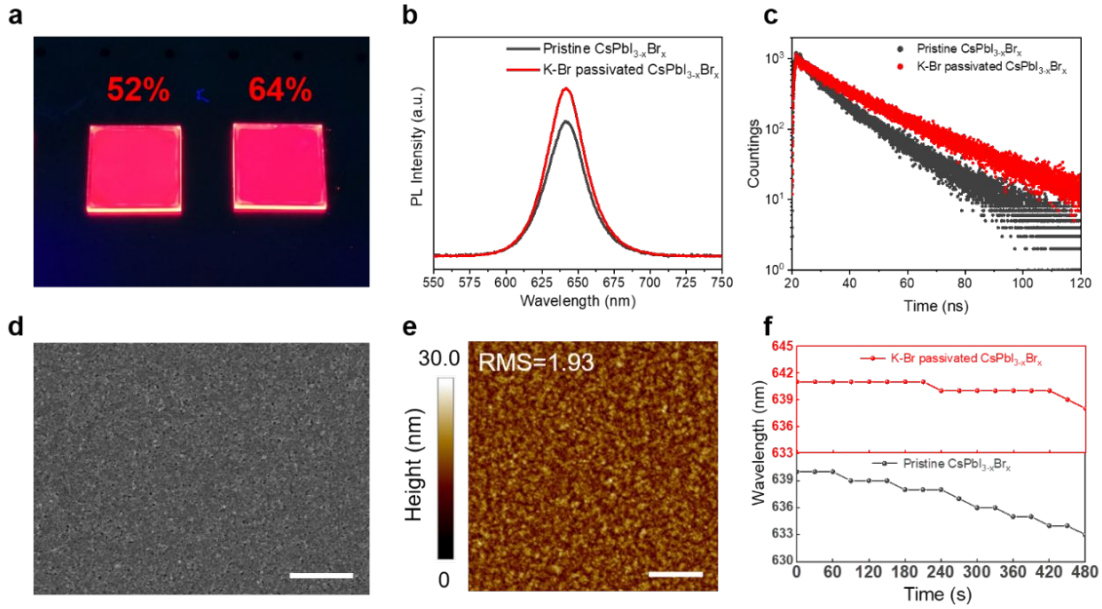

Figure 4. Optical properties and morphologies of $CsPbI_{3-x}Br_x$ NC thin films. (a) Photo of $CsPbI_{3-x}Br_x$ NC thin films under UV-light (365 nm) irradiation. From left to right, the samples are the pristine $CsPbI_{3-x}Br_x$ NC film and K-Br-passivated $CsPbI_{3-x}Br_x$ NC film, respectively. PLQYs of these two samples are 52% and 64%, respectively. (b) PL spectra of the $CsPbI_{3-x}Br_x$ NC films. (c) Time-resolved PL decay curves of $CsPbI_{3-x}Br_x$ NC films. (d) SEM image of K-Br-passivated $CsPbI_{3-x}Br_x$ NC film. Scale bar: 500 nm. (e) AFM image of K-Br-passivated $CsPbI_{3-x}Br_x$ NC film. Scale bar: 1 μm. (f) PL peak position as a function of irradiation time for $CsPbBr_{3-x}I_x$ NC films. The ensemble films were continuously excited by a laser emitting at 365 nm with a power density of 100 mW cm^{-2}.

In addition, the morphologies of different perovskite NC thin films were investigated by scanning electron microscopy (SEM) and atomic force microscopy (AFM). As seen from the SEM image in Figure 4d, the K-Br-passivated $CsPbI_{3-x}Br_x$ NC-based red perovskite NC film is uniformly covered by a number of NCs. However, the pristine $CsPbI_{3-x}Br_x$ NC-based film displays a porous structure with a large number of mesoscopic pores (Figure S19a). The AFM images further confirm the better quality of K-Br-passivated $CsPbI_{3-x}Br_x$ NC thin film. The root-mean-square roughness (RMS) values are 2.43 and 1.93 nm for the pristine $CsPbI_{3-x}Br_x$ NC film (Figure S19b) and K-Br-passivated $CsPbI_{3-x}Br_x$ NC film (Figure 4e), respectively.

High film uniformity will significantly reduce the current leakage and result in high efficiency in the fabricated LEDs.[34]

To show the K-Br-enriched surface passivation effect on suppressing photoinduced halide segregation of $CsPbI_{3-x}Br_x$ NCs, we monitored the PL peak variation of $CsPbI_{3-x}Br_x$ NCs under continuous UV-light (365 nm) irradiation. For both the pristine $CsPbI_{3-x}Br_x$ NC solution and K-Br-passivated $CsPbI_{3-x}Br_x$ NC solution, we observed that almost no PL peak shift occurred even after 1 hour of irradiation at 30 mW cm^{-2} (Figure S20) due to the similar segregation and recovery rate for the initial mixed halide perovskite state in NC solution.[15, 21, 35] However, phase segregation does occur in the mixed halide $CsPbI_{3-x}Br_x$ NC film under laser irradiation.[36] The agglomeration of NCs during the formation of a solid thin film enlarges the carrier diffusion length and consequently increased the rate of phase segregation.[15] We used a laser emitting at 365 nm with a power density of 100 mW cm^{-2} (the power density of 1 sun illumination is 100 mW cm^{-2}) to evaluate the PL spectral stability of the pristine $CsPbI_{3-x}Br_x$ NC film and K-Br-passivated $CsPbI_{3-x}Br_x$ NC film. The PL peak position as a function of irradiation time for the $CsPbBr_{3-x}I_x$ NC films is plotted in Figure 4f (the time-dependent normalized PL spectra are provided in Figure S21). The PL peak of the pristine $CsPbI_{3-x}Br_x$ NC film presents a blueshift from the initial 640 nm towards 633 nm after 480 s continuous laser irradiation. By contrast, the PL peak of K-Br-passivated $CsPbI_{3-x}Br_x$ NC film presents a blueshift from the initial 641 nm towards 638 nm slightly after 480 s irradiation, indicating the better PL spectral stability of the K-Br-passivated $CsPbI_{3-x}Br_x$ NC film. In addition, the occurrence of a blueshift under continuous laser irradiation is 180 s for the K-Br-passivated $CsPbI_{3-x}Br_x$ NC film, while the starting time for the blueshift for the

pristine $CsPbI_{3-x}Br_x$ NC film is as short as 60 s. As reported before, surface defects located on the grain boundary can serve as trapping sites for diffused halide ions, promoting the formation of an iodine-rich domain because of the weaker bond between lead ions and iodine ions. Consequently, the iodide ions are mainly channeled away from the laser excitation area, leading to a higher bandgap for carrier recombination.[13] Thus, passivating the surface defects of $CsPbI_{3-x}Br_x$ NCs with a K-Br-enriched surface can inhibit halide migration and consequently stabilize the PL spectra under laser irradiation.

Performances of $CsPbI_{3-x}Br_x$ NC-based pure red LEDs

We fabricated pure red LEDs using as-fabricated $CsPbI_{3-x}Br_x$ NC films as luminescent layers. As illustrated in Figure 5a, the architecture of the device is composed of a layered structure of ITO/PEDOT:PSS/poly-TPD/$CsPbI_{3-x}Br_x$ NCs/TPBi/LiF/Al, in which ITO serves as the anode, PEDOT:PSS as the hole-injection layer, poly-TPD as the hole-transport layer and electron blocking layer, TPBi as the electron-transport layer, and LiF/Al as the cathode.[37] As shown in the cross-sectional SEM image (Figure 5b), the thicknesses of the PEDOT:PSS, poly-TPD, $CsPbI_{3-x}Br_x$ NCs, TPBi, and LiF/Al layers are ~20, ~40, ~30, ~40 and ~100 nm, respectively. The normalized EL and PL spectra of the K-Br-passivated $CsPbI_{3-x}Br_x$ NC LED are plotted in Figure 5c. The EL spectrum is centered at 637 nm with a narrow FWHM of 31 nm (Figure 5c, solid line), corresponding to the Commission Internationale del'Eclairage (CIE) color coordinates of (0.70, 0.30) (Figure S22). The coordinate of a red channel for displays is (0.71, 0.29), indicating our $CsPbI_{3-x}Br_x$ NCs are an ideal emitter for red displays. The EL peak exhibits a slight blueshift (~4 nm) relative to the PL peak of the corresponding

$CsPbI_{3-x}Br_x$ NC film, which is consistent with the previous reports for the EL variation of perovskite LEDs.[38, 39] A photo of the LED (inset in Figure 5c) shows the bright pure red-light emission of our fabricated LED under an applied voltage of 5 V.

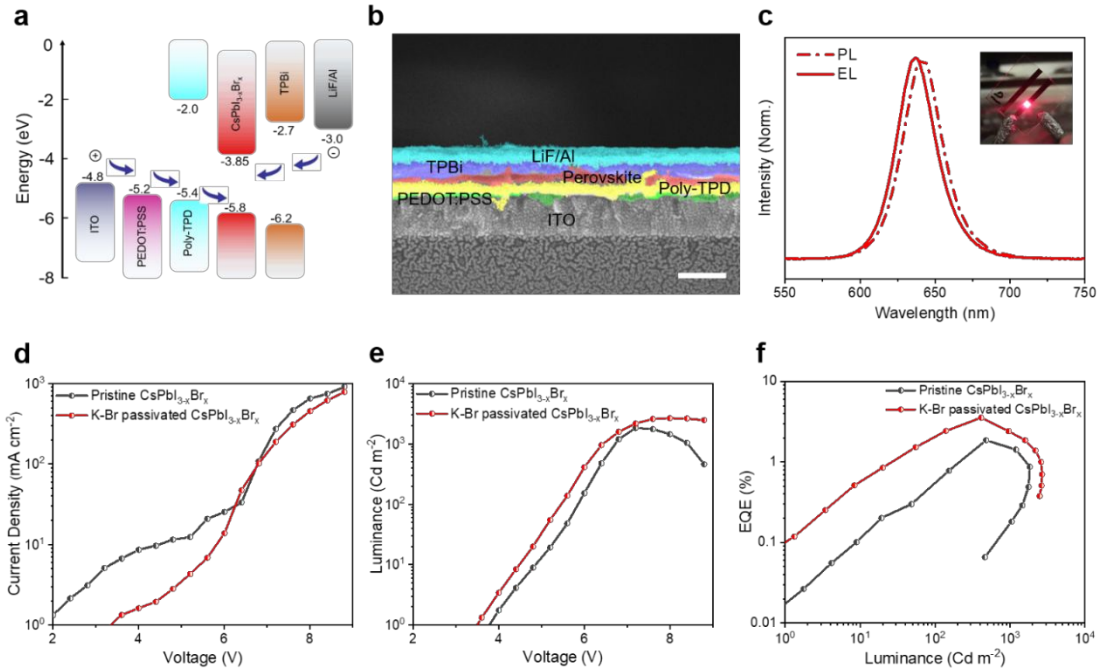

Figure 5. Device characteristics of $CsPbI_{3-x}Br_x$ NC-based pure red LEDs. (a) The energy-level diagram of the LED device structure proposed in this study. (b) Cross-sectional SEM image of the as-fabricated LED device. Scale bar: 200 nm. (c) EL spectrum at an operation voltage of 5 V and the corresponding PL spectrum for the K-Br-passivated $CsPbI_{3-x}Br_x$ NC-based LED. Inset shows the photo of the corresponding device at an applied voltage of 5 V. (d) Current density versus driving voltage curves for LEDs based on prepared $CsPbI_{3-x}Br_x$ NCs. (e) Luminance versus driving voltage curves for LEDs based on prepared $CsPbI_{3-x}Br_x$ NCs. (f) EQEs of LEDs based on prepared $CsPbI_{3-x}Br_x$ NCs at different luminance.

To demonstrate the merits of K-Br-passivated $CsPbI_{3-x}Br_x$ NCs for LEDs, we further compared the performance of $CsPbI_{3-x}Br_x$ NC-based pure red LEDs. The current-density–voltage (*J*–*V*) characteristics of the LEDs are shown in Figure 5d. At the turn-on voltage of the device (3.8 V for pristine $CsPbI_{3-x}Br_x$ NC-based LED and 3.6 V for K-Br-passivated $CsPbI_{3-x}Br_x$ NC-based LED, Figure 5e), the current density of the K-Br-passivated

$CsPbI_{3-x}Br_x$ NC-based LED is lower than that of the pristine $CsPbI_{3-x}Br_x$ NC-based LED, indicating less current leakage of the device based on the K-Br-passivated NC film. The luminance–voltage (*L–V*) curves of the as-fabricated LEDs are presented in Figure 5e. The maximum value of luminance is 2671 cd m^{-2} for K-Br-passivated $CsPbI_{3-x}Br_x$ NC-based devices, which is higher than that of the pristine $CsPbI_{3-x}Br_x$ NCs of 1891 cd m^{-2}. This represents a high value for pure red LEDs emitting at 630 nm ~ 650 nm to date (refer to Table S5). As seen in Figure 5f, the K-Br-passivated $CsPbI_{3-x}Br_x$ NC-based LED reaches a maximum EQE of 3.55%, while the pure $CsPbI_{3-x}Br_x$ NC-based LED reaches a maximum EQE of 1.89%. Additionally, the devices based on K-Br-passivated $CsPbI_{3-x}Br_x$ NCs show an average peak EQE of 3.38% and an average luminance of 2640 Cd m^{-2} (Figure S23) based on the statistics of 30 devices, indicating that the fabrication of our device is reproducible. All the above results indicate that $CsPbI_{3-x}Br_x$ NCs passivated by the K-Br enriched surface present a higher charge injection efficiency and good photoelectric properties, originating from the uniform NC film and well-passivated surface.[40, 41]

EL stability evaluation of $CsPbI_{3-x}Br_x$ NC-based LEDs

To test the EL spectral stability of $CsPbI_{3-x}Br_x$ NC-based pure red LEDs, we measured the emission spectra with the increase in the driving voltages. As shown in Figure 6a, the redshift of the EL peak of the pristine $CsPbI_{3-x}Br_x$ NC-based LED was observed when the driving voltage increased, as shown in previous reports.[11, 12] In contrast, the EL peak of the device based on the K-Br-passivated $CsPbI_{3-x}Br_x$ NCs was maintained at nearly the same position (637 nm) even when the driving voltage increased to 6.0 V (Figure 6b). We correlated the EL peak position with the driving voltage as shown in Figure 6c. The pristine $CsPbI_{3-x}Br_x$

NC-based LED starts to redshift at 4.6 V and the wavelength increase reaches 20 nm when the voltage increased to 6.0 V, while the K-Br-passivated $CsPbI_{3-x}Br_x$ NC-based LED does not exhibit any redshift under 6.0 V, which indicates that the phase segregation caused by ion migration is well suppressed by K-Br passivation. We tested the spectral stability of the fabricated $CsPbI_{3-x}Br_x$ NC-based LEDs under a continuous driving voltage of 5.0 V as well. As shown in Figure 6d, the EL spectra of the LED device based on pristine $CsPbI_{3-x}Br_x$ NCs moves swiftly from 638 nm to 661 nm within 3 min, while the emission peak of the K-Br-passivated $CsPbI_{3-x}Br_x$ NC-based LED moves slowly from 637 nm to 645 nm within 3 min (Figure 6e). In addition, we measured the lifetime of the device by applying a constant voltage and monitoring the evolution of luminance (Figure 6f). The half-lifetime of the pristine $CsPbI_{3-x}Br_x$ NC-based LED is only 30 min, while that of the K-Br-passivated $CsPbI_{3-x}Br_x$ NC-based LED improved to 50 min, indicating the higher stability of our K-Br-passivated $CsPbI_{3-x}Br_x$ NCs.

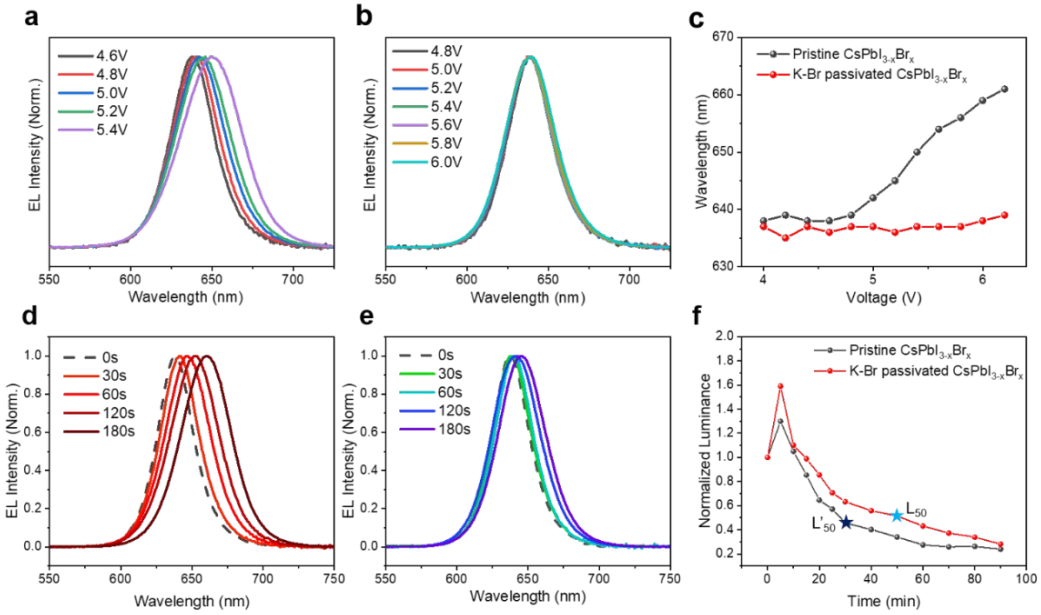

Figure 6. Characteristics of EL stability for $CsPbI_{3-x}Br_x$ NC-based pure red LEDs. (a) Normalized EL spectra of pure red LEDs based on pristine $CsPbI_{3-x}Br_x$ NCs under different

driving voltages. (b) Normalized EL spectra of pure red LEDs based on K-Br-passivated $CsPbI_{3-x}Br_x$ NCs under different driving voltages. (c) EL peak position versus the driving voltage for $CsPbI_{3-x}Br_x$ NC-based pure red LEDs. (d) Normalized EL spectra of the pure red LED based on pristine $CsPbI_{3-x}Br_x$ NCs at a driving voltage of 5.0 V with different times. (e) Normalized EL spectra of the pure red LED based on K-Br-passivated $CsPbI_{3-x}Br_x$ NCs at a driving voltage of 5.0 V with different times. (f) Operation lifetime for the devices based on prepared $CsPbI_{3-x}Br_x$ NCs measured at a constant driving voltage of 5.0 V. The luminance of the LEDs was normalized to their initial values.

Mechanisms for the high EL stability of K-Br-passivated $CsPbI_{3-x}Br_x$ NC-based LEDs

The mechanism for inhibiting ion migration in mixed halide $CsPbI_{3-x}Br_x$ NC-based LEDs passivated by a K-Br enriched surface is discussed here (Scheme. 1). As reported before, the defects in the perovskite grain boundary trap charge carriers and subsequently generate an electric field, further leading to new formation of lower-energy iodide-rich domains.[42] As mentioned above, potassium ion modification should mainly happen on the surface of $CsPbI_{3-x}Br_x$ NCs by bonding with surface bromide ions. On the one hand, potassium ions and bromide ions possess a higher binding energy than lead ions and bromide ions, resulting in a barrier for bromide ions to migrate under an electric field to form halide vacancy defects at the grain boundary. On the other hand, as reported by Abdi-Jalebi et al., potassium ions and bromide ions are more likely to passivate the defects at the grain boundary of the perovskite NC film, consequently, potassium ions and excess halide ions are able to form halide-sequestering species at the grain boundary, immobilizing the halide ions, thereby inhibiting their migration.[19] Thus, halide segregation can be suppressed via K-Br surface passivation by lowering the defect concentration of the grain boundary in perovskite NC films.

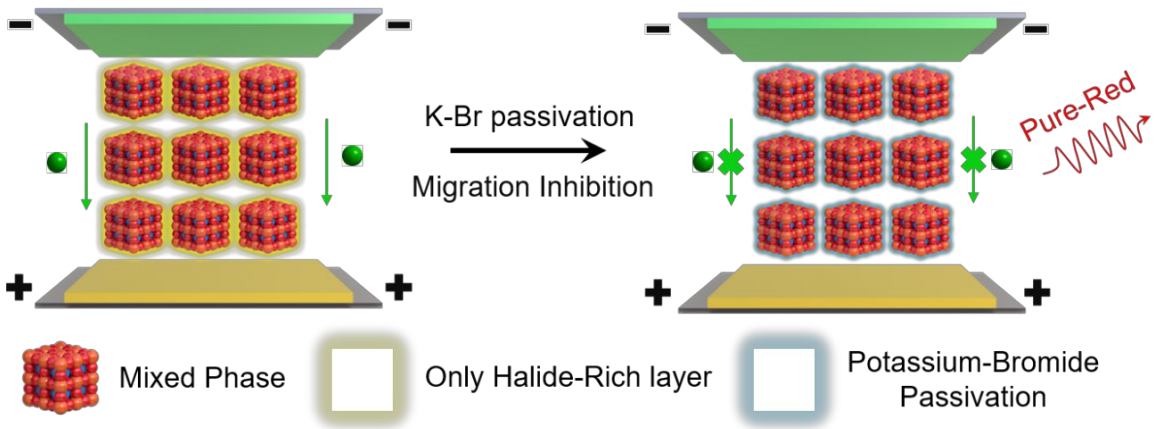

Scheme. 1 Illustration of ion migration suppressed by potassium-bromide-enriched surface passivation.

However, a redshift is still observed in our pure red LEDs because the migration of halide ions in mixed halide perovskite NC films under an electric field has not been totally inhibited. This is therefore a key area that will require a significant focused research effort to resolve.[1] To fabricate color stable pure light emission perovskite LEDs, additional strategies are suggested to be applied in future study: First, substituting Pb^{2+} ions with suitable cations into the B site of the perovskite matrix to increase the crystal formation energy and stabilize the lattice of mixed halide perovskite;[25] second, passivating surface halide vacancies with a thin inorganic crystal layer at the grain boundary of perovskite NCs to block ion migration;[43] and finally, optimizing the LED device structure, especially balancing the electron and the hole injection efficiency to reduce charge accumulation inside the device.[6, 44]

CONCLUSION

We have developed a facile synthetic approach to prepare high-quality $CsPbI_{3-x}Br_x$ NCs emitting at 640 nm with high PLQY (~93%) by potassium-bromide-enriched surface passivation. Moreover, we fabricated pure red LED emitting at 637 nm by using

K-Br-passivated $CsPbI_{3-x}Br_x$ NCs as luminescent layers, which is the desired red emission for next-generation LED displays. The as-fabricated pure red LEDs exhibited a high brightness of 2671 Cd m^{-2} and a relatively high external quantum efficiency of 3.55%. More importantly, the color stability of pure red LEDs based on K-Br-passivated $CsPbI_{3-x}Br_x$ NCs is higher than the one based on pristine $CsPbI_{3-x}Br_x$ NCs, showing great potential for future EL stable pure red LEDs. Our reported K-Br passivation strategy on the surface of mixed halide perovskite NCs will provide an alternative route to fabricate stable and high color pure perovskite LEDs.

ASSOCIATED CONTENT

Supporting Information.

TEM images, energy dispersive X-ray spectroscopy, XPS spectra, PL spectra, PL lifetime, FT-IR spectra, XRD patterns, SEM image, AFM image, photostability test and performance summary of perovskite-based pure red LEDs.

NOTES

The authors declare no competing financial interest.

ACKNOWLEDGEMENT

We acknowledge the funding support from the National Natural Science Foundation of China (Grants 51571184, 21875236, 51872275), the Fundamental Research Funds for the Central Universities (Grant WK2060190085), the joint Funds from Hefei National Synchrotron Radiation Laboratory (Grant KY2060000111), the National Key R&D Program of China (Grant No. 2018YFA0306600) and Anhui Initiative in Quantum Information Technologies (Grant No. AHY050000). This work was partially carried out at the USTC Center for Micro and Nanoscale Research and Fabrication. We thank the Photoemission End-stations (BL10B) at the Hefei National Synchrotron Radiation Laboratory (NSRL) for help in the SRPES characterizations.

REFERENCES

1. Wei, Y.; Cheng, Z. Y.; Lin, J., An Overview on Enhancing the Stability of Lead Halide Perovskite Quantum Dots and Their Applications in Phosphor-Converted LEDs. *Chem. Soc. Rev.* **2019,** *48* (1), 310-350.

2. Akkerman, Q. A.; Raino, G.; Kovalenko, M. V.; Manna, L., Genesis, Challenges and Opportunities for Colloidal Lead Halide Perovskite Nanocrystals. *Nat. Mater.* **2018,** *17* (5), 394-405.

3. Krieg, F.; Ochsenbein, S. T.; Yakunin, S.; ten Brinck, S.; Aellen, P.; Suess, A.; Clerc, B.; Guggisberg, D.; Nazarenko, O.; Shynkarenko, Y.; Kumar, S.; Shih, C. J.; Infante, I.; Kovalenko, M. V., Colloidal $CsPbX_3$ (X = CI, Br, I) Nanocrystals 2.0: Zwitterionic Capping Ligands for Improved Durability and Stability. *ACS Energy Lett.* **2018,** *3* (3), 641-646.

4. Protesescu, L.; Yakunin, S.; Bodnarchuk, M. I.; Krieg, F.; Caputo, R.; Hendon, C. H.; Yang, R. X.; Walsh, A.; Kovalenko, M. V., Nanocrystals of Cesium Lead Halide Perovskites ($CsPbX_3$, X = Cl, Br, and I): Novel Optoelectronic Materials Showing Bright Emission with Wide Color Gamut. *Nano Lett.* **2015,** *15* (6), 3692-3696.

5. Nedelcu, G.; Protesescu, L.; Yakunin, S.; Bodnarchuk, M. I.; Grotevent, M. J.; Kovalenko, M. V., Fast Anion-Exchange in Highly Luminescent Nanocrystals of Cesium Lead Halide Perovskites ($CsPbX_3$, X = Cl, Br, I). *Nano Lett.* **2015,** *15* (8), 5635-5640.

6. Lin, K. B.; Xing, J.; Quan, L. N.; de Arquer, F. P. G.; Gong, X. W.; Lu, J. X.; Xie, L. Q.; Zhao, W. J.; Zhang, D.; Yan, C. Z.; Li, W. Q.; Liu, X. Y.; Lu, Y.; Kirman, J.; Sargent, E. H.; Xiong, Q. H.; Wei, Z. H., Perovskite Light-Emitting Diodes with External Quantum Efficiency Exceeding 20 Percent. *Nature* **2018,** *562* (7726), 245.

7. Chiba, T.; Hayashi, Y.; Ebe, H.; Hoshi, K.; Sato, J.; Sato, S.; Pu, Y. J.; Ohisa, S.; Kido, J., Anion-Exchange Red Perovskite Quantum Dots with Ammonium Iodine Salts for Highly Efficient Light-Emitting Devices. *Nat. Photon.* **2018,** *12* (11), 681-687.

8. Xu, W. D.; Hu, Q.; Bai, S.; Bao, C. X.; Miao, Y. F.; Yuan, Z. C.; Borzda, T.; Barker, A. J.; Tyukalova, E.; Hu, Z. J.; Kawecki, M.; Wang, H. Y.; Yan, Z. B.; Liu, X. J.; Shi, X. B.; Uvdal, K.; Fahlman, M.; Zhang, W. J.; Duchamp, M.; Liu, J. M.; Petrozza, A.; Wang, J. P.; Liu, L. M.; Huang, W.; Gao, F., Rational Molecular Passivation for High-Performance Perovskite Light-Emitting Diodes. *Nat. Photon.* **2019,** *13* (6), 418-424.

9. Hassan, Y.; Ashton, O. J.; Park, J. H.; Li, G. R.; Sakai, N.; Wenger, B.; Haghighirad, A. A.; Noel, N. K.; Song, M. H.; Lee, B. R.; Friend, R. H.; Snaith, H. J., Facile Synthesis of Stable and Highly Luminescent Methylammonium Lead Halide Nanocrystals for Efficient Light Emitting Devices. *J. Am. Chem. Soc.* **2019,** *141* (3), 1269-1279.

10. Zhu, R. D.; Luo, Z. Y.; Chen, H. W.; Dong, Y. J.; Wu, S. T., Realizing Rec. 2020 Color Gamut with Quantum Dot Displays. *Opt. Express* **2015,** *23* (18), 23680-23693.

11. Vashishtha, P.; Halpert, J. E., Field-Driven Ion Migration and Color Instability in Red-Emitting Mixed Halide Perovskite Nanocrystal Light-Emitting Diodes. *Chem. Mater.* **2017,** *29* (14), 5965-5973.

12. Wang, K. H.; Peng, Y. D.; Ge, J.; Jiang, S. L.; Zhu, B. S.; Yao, J. S.; Yin, Y. C.; Yang, J. N.; Zhang, Q.; Yao, H. B., Efficient and Color-Tunable Quasi-2D $CsPbBr_xCl_{3-x}$ Perovskite Blue Light-Emitting Diodes. *ACS Photon.* **2019,** *6* (3), 667-676.

13. Zhang, H. C.; Fu, X.; Tang, Y.; Wang, H.; Zhang, C. F.; Yu, W. W.; Wang, X. Y.; Zhang, Y.; Xiao, M., Phase Segregation due to Ion Migration in All-Inorganic Mixed-Halide Perovskite Nanocrystals. *Nat. Commun.* **2019,** *10*, 1088.

14. Samu, G. F.; Balog, A.; De Angelis, F.; Meggiolaro, D.; Kamat, P. V.; Janaky, C., Electrochemical Hole

Injection Selectively Expels Iodide from Mixed Halide Perovskite Films. *J. Am. Chem. Soc.* **2019,** *141* (27), 10812-10820.

15. Draguta, S.; Sharia, O.; Yoon, S. J.; Brennan, M. C.; Morozov, Y. V.; Manser, J. S.; Kamat, P. V.; Schneider, W. F.; Kuno, M., Rationalizing the Light-Induced Phase Separation of Mixed Halide Organic-Inorganic Perovskites. *Nat. Commun.* **2018,** *9*, 200.

16. Gualdrón Reyes A F; Yoon S J; Mora-Sero I, Recent Insights for Achieving Mixed Halide Perovskites without Halide Segregation. *Curr. Opin. Electrochem.* **2018,** *11*, 84-90.

17. Yi, C. Y.; Luo, J. S.; Meloni, S.; Boziki, A.; Ashari-Astani, N.; Gratzel, C.; Zakeeruddin, S. M.; Rothlisberger, U.; Gratzel, M., Entropic Stabilization of Mixed A-Cation ABX_3 Metal Halide Perovskites for High Performance Perovskite Solar Cells. *Energy Environ. Sci.* **2016,** *9* (2), 656-662.

18. Yang, Z. B.; Rajagopal, A.; Jo, S. B.; Chueh, C. C.; Williams, S.; Huang, C. C.; Katahara, J. K.; Hillhouse, H. W.; Jen, A. K. Y., Stabilized Wide Bandgap Perovskite Solar Cells by Tin Substitution. *Nano Lett.* **2016,** *16* (12), 7739-7747.

19. Abdi-Jalebi, M.; Andaji-Garmaroudi, Z.; Cacovich, S.; Stavrakas, C.; Philippe, B.; Richter, J. M.; Alsari, M.; Booker, E. P.; Hutter, E. M.; Pearson, A. J.; Lilliu, S.; Savenije, T. J.; Rensmo, H.; Divitini, G.; Ducati, C.; Friend, R. H.; Stranks, S. D., Maximizing and Stabilizing Luminescence from Halide Perovskites with Potassium Passivation. *Nature* **2018,** *555* (7697), 497-501.

20. Yang, D.; Li, X.; Wu, Y.; Wei, C.; Qin, Z.; Zhang, C.; Sun, Z.; Li, Y.; Wang, Y.; Zeng, H., Surface Halogen Compensation for Robust Performance Enhancements of $CsPbX_3$ Perovskite Quantum Dots. *Adv. Opt. Mater.* **2019,** *7* (11), 1900276.

21. Gualdron-Reyes, A. F.; Yoon, S. J.; Barea, E. M.; Agouram, S.; Munoz-Sanjose, V.; Melendez, A. M.; Nino-Gomez, M. E.; Mora-Sero, I., Controlling the Phase Segregation in Mixed Halide Perovskites through Nanocrystal Size. *ACS Energy Lett.* **2019,** *4* (1), 54-62.

22. Huang, S. Q.; Wang, B.; Zhang, Q.; Li, Z. C.; Shan, A. D.; Li, L., Postsynthesis Potassium-Modification Method to Improve Stability of $CsPbBr_3$ Perovskite Nanocrystals. *Adv. Opt. Mater.* **2018,** *6* (6), 1701106.

23. Creutz, S. E.; Crites, E. N.; De Siena, M. C.; Gamelin, D. R., Anion Exchange in Cesium Lead Halide Perovskite Nanocrystals and Thin Films Using Trimethylsilyl Halide Reagents. *Chem. Mater.* **2018,** *30* (15), 4887-4891.

24. Cai, Y. T.; Wang, H. R.; Li, Y.; Wang, L.; Lv, Y.; Yang, X. Y.; Xie, R. J., Trimethylsilyl Iodine-Mediated Synthesis of Highly Bright Red-Emitting $CsPbI_3$ Perovskite Quantum Dots with Significantly Improved Stability. *Chem. Mater.* **2019,** *31* (3), 881-889.

25. Zhang, J.; Zhang, L.; Cai, P.; Xue, X.; Wang, M.; Zhang, J.; Tu, G., Enhancing Stability of Red Perovskite Nanocrystals Through Copper Substitution for Efficient Light-Emitting Diodes. *Nano Energy* **2019,** *62*, 434-441.

26. Yao, J. S.; Ge, J.; Wang, K. H.; Zhang, G. Z.; Zhu, B. S.; Chen, C.; Zhang, Q.; Luo, Y.; Yu, S. H.; Yao, H. B., Few-Nanometer-Sized α-$CsPbI_3$ Quantum Dots Enabled by Strontium Substitution and Iodide Passivation for Efficient Red-Light Emitting Diodes. *J. Am. Chem. Soc.* **2019,** *141* (5), 2069-2079.

27. Tao, F.; Grass, M. E.; Zhang, Y. W.; Butcher, D. R.; Renzas, J. R.; Liu, Z.; Chung, J. Y.; Mun, B. S.; Salmeron, M.; Somorjai, G. A., Reaction-Driven Restructuring of Rh-Pd and Pt-Pd Core-Shell Nanoparticles. *Science* **2008,** *322* (5903), 932-934.

28. Wagner, C. D.; Taylor, J. A., Generation of XPS Auger Lines by Bremsstrahlung. *J. Electron. Spectrosc. Relat. Phenom.* **1980,** *20* (1-2), 83-93.

29. Yao, J. S.; Ge, J.; Han, B. N.; Wang, K. H.; Yao, H. B.; Yu, H. L.; Li, J. H.; Zhu, B. S.; Song, J. Z.; Chen, C.; Zhang, Q.; Zeng, H. B.; Luo, Y.; Yu, S. H., Ce^{3+}-Doping to Modulate Photoluminescence Kinetics for Efficient $CsPbBr_3$ Nanocrystals Based Light-Emitting Diodes. *J. Am. Chem. Soc.* **2018,** *140* (10), 3626-3634.

30. Pan, J.; Quan, L. N.; Zhao, Y. B.; Peng, W.; Murali, B.; Sarmah, S. P.; Yuan, M. J.; Sinatra, L.; Alyami, N. M.; Liu, J. K.; Yassitepe, E.; Yang, Z. Y.; Voznyy, O.; Comin, R.; Hedhili, M. N.; Mohammed, O. F.; Lu, Z. H.; Kim, D. H.; Sargent, E. H.; Bakr, O. M., Highly Efficient Perovskite-Quantum-Dot Light-Emitting Diodes by Surface Engineering. *Adv. Mater.* **2016,** *28* (39), 8718-8725.

31. Tang, J.; Kemp, K. W.; Hoogland, S.; Jeong, K. S.; Liu, H.; Levina, L.; Furukawa, M.; Wang, X. H.; Debnath, R.; Cha, D. K.; Chou, K. W.; Fischer, A.; Amassian, A.; Asbury, J. B.; Sargent, E. H., Colloidal-Quantum-Dot Photovoltaics Using Atomic-Ligand Passivation. *Nat. Mater.* **2011,** *10* (10), 765-771.

32. Song, J. Z.; Li, J. H.; Xu, L. M.; Li, J. H.; Zhang, F. J.; Han, B. N.; Shan, Q. S.; Zeng, H. B., Room-Temperature Triple-Ligand Surface Engineering Synergistically Boosts Ink Stability, Recombination Dynamics, and Charge Injection toward EQE-11.6% Perovskite QLEDs. *Adv. Mater.* **2018,** *30* (30), 1800764.

33. deQuilettes, D. W.; Koch, S.; Burke, S.; Paranji, R. K.; Shropshire, A. J.; Ziffer, M. E.; Ginger, D. S., Photoluminescence Lifetimes Exceeding 8 μs and Quantum Yields Exceeding 30% in Hybrid Perovskite Thin Films by Ligand Passivation. *ACS Energy Lett.* **2016,** *1* (2), 438-444.

34. Gangishetty, M. K.; Sanders, S. N.; Congreve, D. N., Mn^{2+} Doping Enhances the Brightness, Efficiency, and Stability of Bulk Perovskite Light-Emitting Diodes. *ACS Photon.* **2019,** *6* (5), 1111-1117.

35. Bischak, C. G.; Hetherington, C. L.; Wu, H.; Aloni, S.; Ogletree, D. F.; Limmer, D. T.; Ginsberg, N. S., Origin of Reversible Photoinduced Phase Separation in Hybrid Perovskites. *Nano Lett.* **2017,** *17* (2), 1028-1033.

36. Dequilettes, D. W.; Zhang, W.; Burlakov, V. M.; Graham, D. J.; Leijtens, T.; Osherov, A.; Bulovic, V.; Snaith, H. J.; Ginger, D. S.; Stranks, S. D., Photo-Induced Halide Redistribution in Organic-Inorganic Perovskite Films. *Nat. Commun.* **2016,** *7*, 11683.

37. Liu, P. Z.; Chen, W.; Wang, W. G.; Xu, B.; Wu, D.; Hao, J. J.; Cao, W. Y.; Fang, F.; Li, Y.; Zeng, Y. Y.; Pan, R. K.; Chen, S. M.; Cao, W. Q.; Sun, X. W.; Wane, K., Halide-Rich Synthesized Cesium Lead Bromide Perovskite Nanocrystals for Light-Emitting Diodes with Improved Performance. *Chem. Mater.* **2017,** *29* (12), 5168-5173.

38. Zhu, B. S.; Li, H. Z.; Ge, J.; Li, H. D.; Yin, Y. C.; Wang, K. H.; Chen, C.; Yao, J. S.; Zhang, Q.; Yao, H. B., Room Temperature Precipitated Dual Phase $CsPbBr_3$-$CsPb_2Br_5$ Nanocrystals for Stable Perovskite Light Emitting Diodes. *Nanoscale* **2018,** *10* (41), 19262-19271.

39. Xu, J. W.; Huang, W. X.; Li, P. Y.; Onken, D. R.; Dun, C. C.; Guo, Y.; Ucer, K. B.; Lu, C.; Wang, H. Z.; Geyer, S. M.; Williams, R. T.; Carroll, D. L., Imbedded Nanocrystals of $CsPbBr_3$ in Cs_4PbBr_6: Kinetics, Enhanced Oscillator Strength, and Application in Light-Emitting. *Adv. Mater.* **2017,** *29* (43), 1703703.

40. Xiao, Z. G.; Kerner, R. A.; Zhao, L. F.; Tran, N. L.; Lee, K. M.; Koh, T. W.; Scholes, G. D.; Rand, B. P., Efficient Perovskite Light-Emitting Diodes Featuring Nanometre-Sized Crystallites. *Nat. Photon.* **2017,** *11* (2), 108-115.

41. Zhang, L. Q.; Yang, X. L.; Jiang, Q.; Wang, P. Y.; Yin, Z. G.; Zhang, X. W.; Tan, H. R.; Yang, Y.; Wei, M. Y.; Sutherland, B. R.; Sargent, E. H.; You, J. B., Ultra-Bright and Highly Efficient Inorganic Based Perovskite Light-Emitting Diodes. *Nat. Commun.* **2017,** *8*, 15640.

42. Knight, A. J.; Wright, A. D.; Patel, J. B.; McMeekin, D. P.; Snaith, H. J.; Johnston, M. B.; Herz, L. M., Electronic Traps and Phase Segregation in Lead Mixed-Halide Perovskite. *ACS Energy Lett.* **2019,** *4* (1), 75-84.

43. Dirin, D. N.; Benin, B. M.; Yakunin, S.; Krumeich, F.; Raino, G.; Frison, R.; Kovalenko, M. V., Microcarrier-Assisted Inorganic Shelling of Lead Halide Perovskite Nanocrystals. *ACS Nano* **2019,** *13* (10), 11642-11652.

44. Shi, Y. F.; Wu, W.; Dong, H.; Li, G. R.; Xi, K.; Divitini, G.; Ran, C. X.; Yuan, F.; Zhang, M.; Jiao, B.; Hou, X.; Wu, Z. X., A Strategy for Architecture Design of Crystalline Perovskite Light-Emitting Diodes with High Performance. *Adv. Mater.* **2018,** *30* (25), 1800251.

Artwork for TOC